Global Environmental Science
www.sciltp.com/journals/ges

Article

Size Distribution and Source Apportionment of Trace Metal Elements in the Atmospheric Aerosols in a Coastal City, Northern China

Ziyan Xi [1,2], Jianhua Qi [3,4,*], Yuanzhe Ni [1,3], Zengjie Zuo [5] and Xuehui Lin [6]

1 College of Environmental Science and Engineering, Ocean University of China, Qingdao 266100, China
2 Zhonghuan Qiyan (Beijing) Low Carbon Technology Co., Ltd., Beijing 100012, China
3 Key Laboratory of Marine Environment and Ecology, Ministry of Education, Ocean University of China, Qingdao 266100, China
4 Laboratory for Marine Ecology and Environmental Science, Qingdao Marine Science and Technology Center, Qingdao 266237, China
5 Institute of Technical Information for Building Materials Industry, Beijing 100024, China
6 Qingdao Institute of Marine Geology, Qingdao 266100, China
* Correspondence: qjianhua@ouc.edu.cn

How To Cite: Xi, Z.; Qi, J.; Ni, Y.; et al. Size Distribution and Source Apportionment of Trace Metal Elements in the Atmospheric Aerosols in a Coastal City, Northern China. *Glob. Environ. Sci.* **2026**, *2*(2), 145–171. https://doi.org/10.53941/ges.2026.100011

Table S1. The size distribution of metals in coastal and inland regions.

Region		Metals	Size distribution	Reference
Coastal region	Qingdao, China	Al, Fe, Mg, Na	Unimodal size distribution with a peak at 3.3–4.7 μm	[1]
		K, Cu	Bimodal distribution, with peaks at 0.43–0.65 μm and 3.3–4.7 μm	
		Pb, Cd	Unimodal size distribution with a peak at 0.43–0.65 μm	
	Cochin, coast of tropical India	Al, Fe, Ti, Ba, Co	Unimodal size distribution with a peak at coarse mode (>2.0 μm)	[2]
		Cu, Zn, Cd, Pb	Unimodal size distribution with a peak at fine mode (<2.0 μm)	
	Kanazawa, Japan	Ca, Mg, Mn, Co, Fe	Dominated in coarse particles with peak at 3.3–4.7 μm (Fe: 4.7–7.0 μm; Co: 7.0–11 μm)	[3]
		Zn, Ba, Cd, Pb, Cu	Dominated in fine particles with peak at 0.65–1.1 μm (Ba: 1.1–2.1 μm; Zn: 0.65–3.3 μm)	
	Antarctic Peninsula	Fe	Unimodal size distribution with a peak at 4.4 μm	[4]
	Tianjin, China	Pb, Cd	Unimodal size distribution with a peak at 0.43–2.1 μm	[5]
		Mn	Unimodal size distribution with a peak at 2.1–4.7 μm	
		Cr, Co	Bimodal distribution, with peaks at 0.43–0.65 μm and 3.3–4.7 μm	
	Taiwan	Al, Fe, Mg	Unimodal size distribution with a peak at 3.2–5.6 μm	[6]
		Ba, Pb, Zn	The primary and secondary peaks for Pb at 1.0–1.8 μm and 18–32 nm; those of Ba in 3.2–5.6 μm and 32–56 nm, and those of Zn were at 1.0–1.8 μm and 32–56 nm	
		Mn, Cu, Cd	Mn exhibited a primary peak at 3.2–5.6 μm and a secondary peak at 1.0–1.8 μm; the peaks of Cu at 0.56–1.0 and 3.2–5.6 μm; those of Cd in 5.6–10 μm and 10–18 nm	
		K	Trimodal size distribution at 0.18–0.32 μm, 0.56–1.0 μm, and 3.2–5.6 μm, respectively	
Inland region	Beijing, China	Fe, Mg	Unimodal size distribution with a peak at 3.3–5.8 μm	[7]
		K, Pb, Cd	Unimodal size distribution with a peak at 0.65–1.1 μm	
		Cu	Bimodal distribution, with peaks at 0.65–1.1 μm and 3.3–5.8 μm	
	Xinglong Base Station, China	Al, Fe, Cr, Co, Cu, Zn, Pb, K	A main peak in 4.7–5.8 μm, with a minor one in 0.43–0.65 μm	[8]
	Central England and southern Scotland	Fe, Ba	With a large mode at or near 3–4 μm	[9]
		Zn, Cu, Co, Mn	With several modes throughout the size range and more evenly distributed mass (peak at 0.4–0.5 μm and 3–5 μm)	
		Cd, Pb	A large mode at or near 0.5 μm	
	Cangzhou, China	Fe	Unimodal size distribution with a peak at 2.1–4.7 μm	[10]
		Cu, Mn	Cu and Mn showed primary peak in 4.7–5.8 μm and secondary peak at 0.43–0.65 and 0.65–1.1 μm, respectively	
		Pb, Zn	Pb and Zn showed primary peak at 0.43–0.65 μm and 0.65–2.1 μm, respectively and minor peak in 4.7–5.8 μm	
	Taishan, China	Mg, Al, Fe, Mn, Ba	A peak concentration in the size range of 4.7–5.8 μm	[11]
		Co, Na, Cu	A bimodal distribution with peak at 4.7–5.8 μm and 0.43–0.65 μm, respectively	
		Zn, Pb	A bimodal distribution with peak at 0.43–1.1 μm and 4.7–5.8 μm	

Table S2. Detection limits, precisions and recoveries of metal elements and water-soluble ions.

Component	Measurement Method	Detection Limit (μg/L)	Precision (RSD %)	Recovery (%)
Li	ICP-MS	0.020	3.7	97.0
Sc		0.060	2.4	97.0
Cr		0.011	3.0	95.0
Co		0.005	3.8	103
Cu		0.022	4.0	106
Zn		0.016	2.5	102
Cd		0.002	5.0	105
Pb		0.034	3.9	104
Al	ICP-AES	7.9	0.60	103
Fe		2.6	0.70	104
Ti		3.0	3.0	
K		10.0	0.79	99.2
Mn		3.0	0.46	98.0
Na		9.0	0.60	99.0
Ba		2.0	3.0	98.2
F^-	IC	1.4	2.8	115
Cl^-		0.80	1.6	109
Br^-		2.1	2.7	93.7
NO_2^-		2.2	2.1	116
NO_3^-		2.7	1.5	96.7
SO_4^{2-}		1.6	1.6	97.7
PO_4^{3-}		13	1.4	95.2
Li^+		0.75	1.3	97.0
Na^+		0.48	0.97	97.8
NH_4^+		0.24	1.1	115
K^+		0.40	1.3	97.5
Mg^{2+}		0.74	1.09	93.0
Ca^{2+}		0.44	0.79	93.6

Table S3. Performance evaluation of the PMF reconstruction: linear regression and Kolmogorov-Smirnov (KS) test between measured and reconstructed concentrations.

Species	Intercept	Slope	SE	R^2	KS Test Stat	KS Test *P* Value
NO_3^-	2.7490	0.4828	2.5418	0.8271	0.1291	0.6410
SO_4^{2-}	2.8100	0.4372	2.4126	0.6803	0.1285	0.6467
NH_4^+	−0.8689	1.0045	4.0000	0.6387	0.0949	0.9277
Cl^-	0.8019	0.5855	0.9890	0.5622	0.0700	0.9970
Al	0.2941	0.7227	0.4122	0.9789	0.1065	0.8485
Ba	−0.0028	1.0173	0.0084	0.9369	0.0928	0.9387
Cd	0.0002	0.7013	0.0003	0.9213	0.1207	0.7221
Co	0.0000	0.8866	0.0001	0.9820	0.0898	0.9529
Cr	0.0004	0.8388	0.0026	0.8052	0.1110	0.8108
Fe	0.2904	0.7749	0.3840	0.9462	0.1193	0.7354
Cu	0.0060	0.4258	0.0049	0.5686	0.1009	0.8901
K	0.0594	0.8005	0.1836	0.9618	0.0898	0.9528
Li	−0.0002	1.0221	0.0009	0.9146	0.1121	0.8013
Mn	0.0069	0.8191	0.0095	0.9517	0.1208	0.7217
Na	0.0344	0.7742	0.2617	0.7210	0.2076	0.1163
Pb	0.0072	0.6305	0.0133	0.7545	0.0840	0.9740
Ti	−0.0184	1.2357	0.0447	0.9868	0.2009	0.1393
Zn	0.0562	0.7478	0.1104	0.8038	0.1566	0.3933
PM	−7.3153	1.0527	16.7427	0.9642	0.1195	0.7336

https://doi.org/10.53941/ges.2026.100011

Table S4. Mapping of bootstrap factors to base factors.

	Factor 1	Factor 2	Factor 3	Factor 4	Factor 5	Factor 6	Unmapped
Boot Factor 1	162	2	8	4	4	5	0
Boot Factor 2	3	180	1	0	1	0	0
Boot Factor 3	0	3	176	4	0	2	0
Boot Factor 4	0	4	1	176	0	4	0
Boot Factor 5	2	1	14	5	154	9	0
Boot Factor 6	4	3	15	15	2	146	0

Table S5. Summary of BS-DISP diagnostics from the PMF error estimation run.

Metric	Value
# of Cases Accepted	299
% of Cases Accepted	60%
Largest Decrease in Q	−9.261
%dQ (percent change in Q)	−0.997956%
# of Decreases in Q	0
# of Swaps in Best Fit	141
# of Swaps in DISP	60
Swaps by Factor (F1–F6)	125, 24, 131, 7, 13, 25

Table S6. PM_{10} emission data in Shandong province from MEIC—China air pollutants emission database (Geng et al. [12]; last update: 2025-11-01, Unit: 10^6 g/season).

Sector		Spring (Mar.-May)	Summer (June-Aug.)	Fall (Sep.-Nov.)	Winter (Dec.-Feb.)
Power	**Power**	23,388.155	25,058.133	23,570.303	22,768.158
Industry	**Heating**	12,838.122	12,280.074	12,187.726	13,404.939
	Industrial boiler	10,033.683	9137.112	9716.75	11,297.509
	Cement	30,260.035	30,474.016	31,357.055	19,105.159
	Coking	12,808.024	13,127.998	13,541.138	13,367.778
	Iron and steel	32,348.128	32,182.58	31,642.592	30,094.545
	Petrochemical	16,351.47	18,150.957	17,074.213	15,633.679
	Oil and gas	0	0	0	0
	Printing	0	0	0	0
	Industry paint use	0	0	0	0
	Architecture paint use	0	0	0	0
	Other industries	69,946.942	70,544.096	68,285.447	58,759.527
Residential	**Residential coal combustion**	23,002.788	13,449.74	23,334.716	52,247.318
	Residential biofuel combustion	21,723.049	21,380.883	22,001.127	46,491.969
	Domestic solvent use	0	0	0	0
	Other residential	28.113	21.017	27.652	82.304
Transportation	**Gasoline vehicle**	356.959	371.143	361.53	364.417
	Diesel vehicle	3546.272	3269.15	3622.413	2695.222
	Motorcycle	1233.294	1304.621	1252.142	1273.364
	Off-road mobile source	11,518.623	11,518.623	11,518.623	11,518.623
Agriculture	**Fertilizer**	0	0	0	0
	Livestock	0	0	0	0
Seasonal Total		269,383.657	262,270.143	26,9493.427	299,104.511

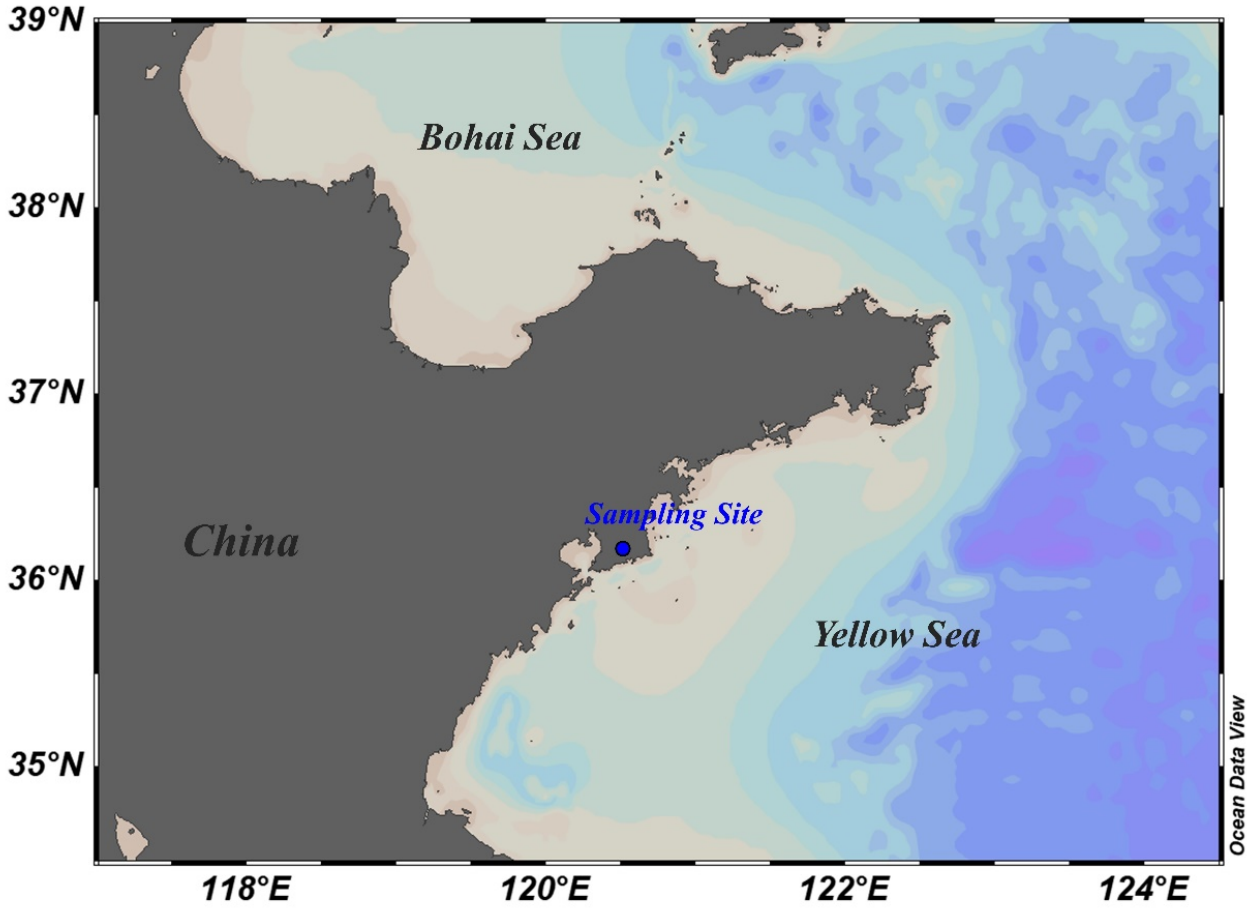

Figure S1. The sampling location.

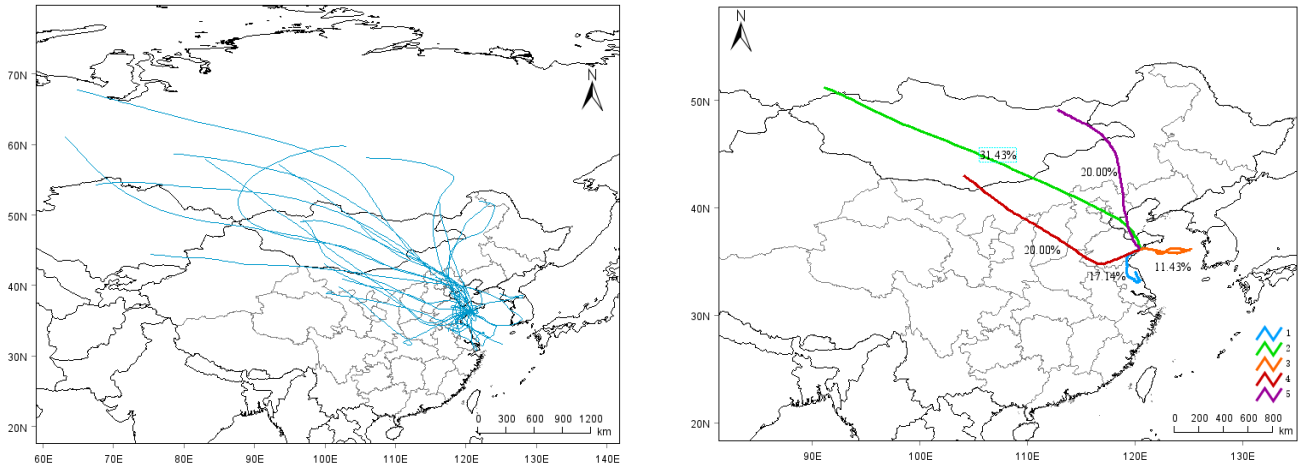

Figure S2. Backward trajectories for samples (**Left**: all samples; **Right**: clustered trajectories. Cluster 1: air mass from southern China with the lowest average transport speed of 7.9 km/h; Cluster 2: air mass from northern China and Siberia with fast transport velocity of 44.5 km/h; Cluster 3: ocean-originated air mass with velocity of 10.7 km/h; Cluster 4: air mass from northwest China with low velocity 24.7 km/h; Cluster 5: air mass from northern China with velocity of 19.6 km/h).

 https://doi.org/10.53941/ges.2026.100011

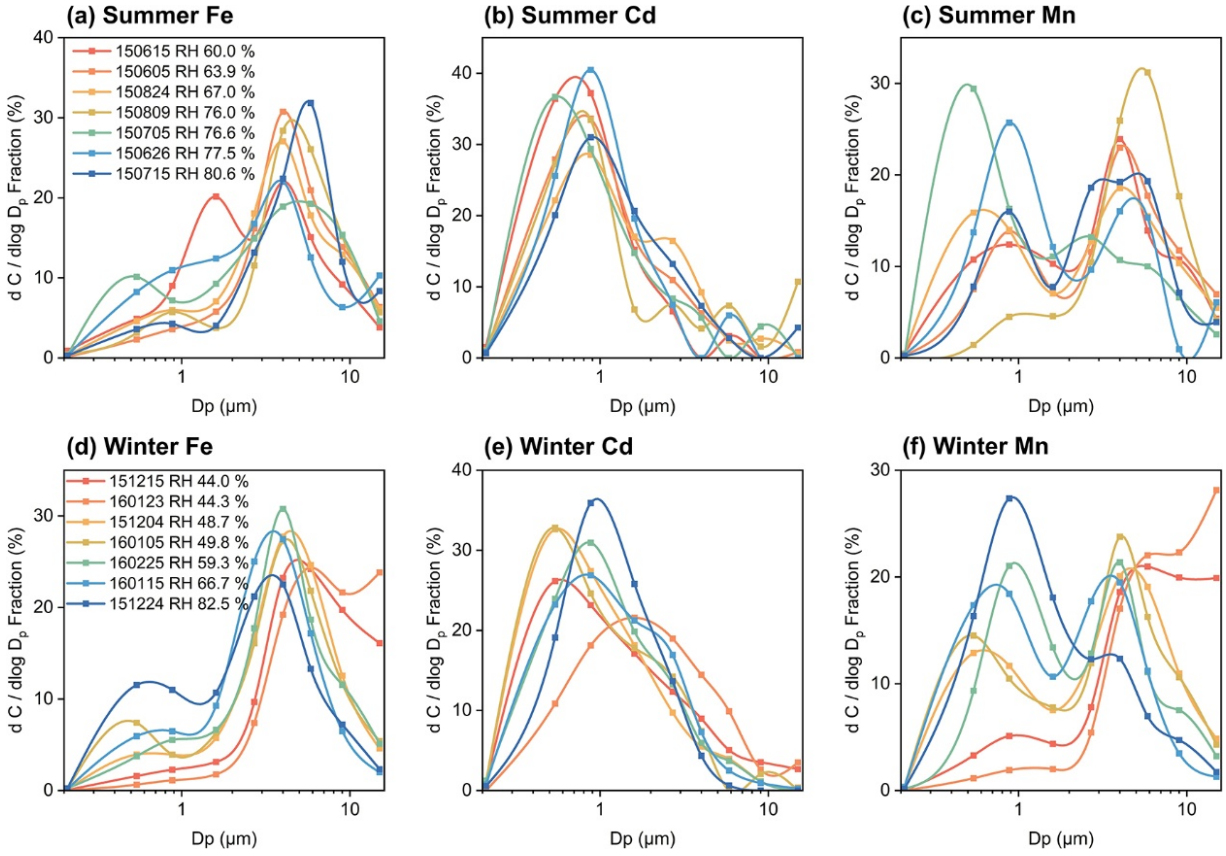

Figure S3. Seasonal (summer/winter) variations in size distributions of Fe, Cd, and Mn under different relative humidity conditions.

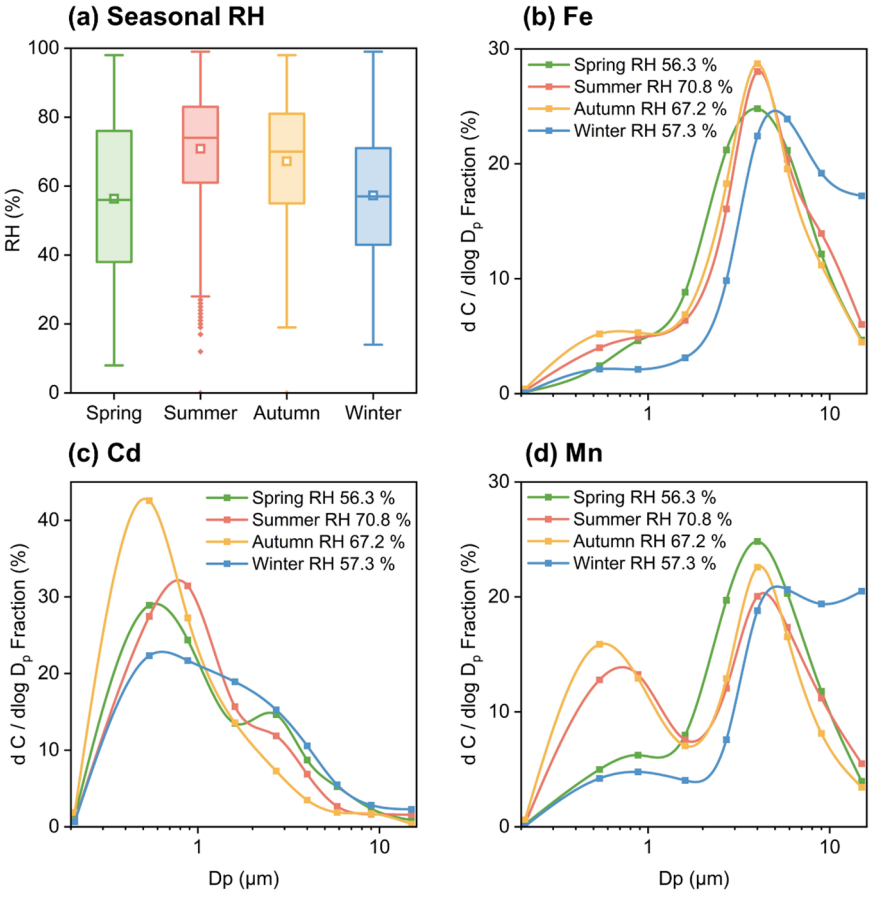

Figure S4. Seasonal variations in relative humidity and size distributions of Fe, Cd, and Mn in Qingdao.

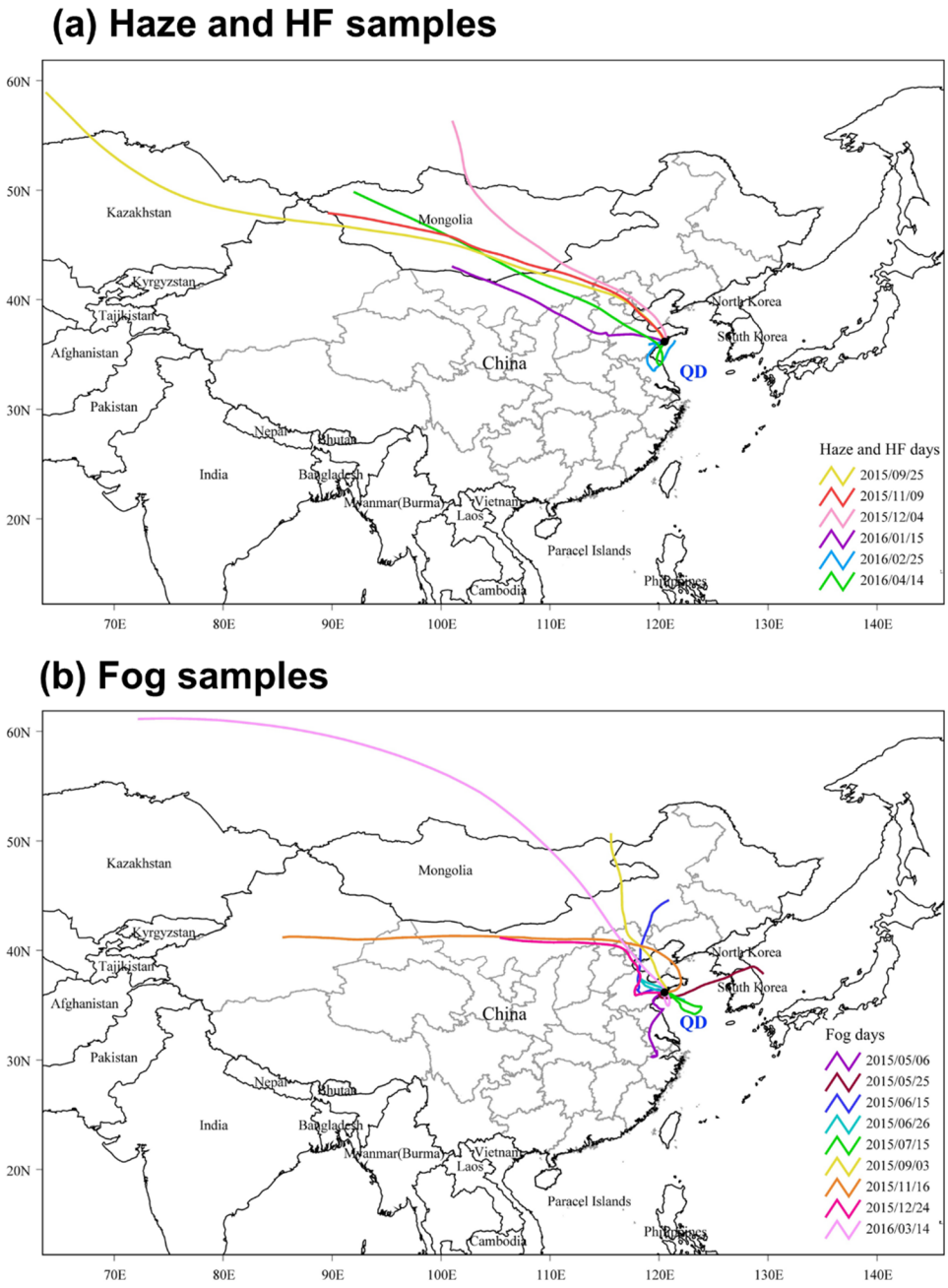

Figure S5. Backward trajectories for samples (**a**) Haze and HF samples; (**b**) Fog samples.

Reference

1. Jin, T.; Qi, J.; Xi, Z.; et al. Impact of a Dust Event on the Size Distribution of Metal Elements in Atmospheric Aerosols at the Coastal Region and over the Ocean. *Environ. Sci.* **2019**, *40*, 1562–1574. (in Chinese)
2. Boreddy, S.K.R.; Hegde, P.; Aswini, A.R. Geochemical Characteristics of Trace Elements in Size-Resolved Coastal Urban Aerosols Associated with Distinct Air Masses over Tropical Peninsular India: Size Distributions and Source Apportionment. *Sci. Total Environ.* **2021**, *763*, 142967.
3. Wang, X.; Sato, T.; Xing, B. Size Distribution and Anthropogenic Sources Apportionment of Airborne Trace Metals in Kanazawa, Japan. *Chemosphere* **2006**, *65*, 2440–2448.
4. Gao, Y.; Yu, S.; Sherrell, R.M.; et al. Particle-Size Distributions and Solubility of Aerosol Iron Over the Antarctic Peninsula during Austral Summer. *J. Geophys. Res. Atmos.* **2020**, *125*, e2019JD032082.
5. Xue, Q.; Liu, X.; Tian, Y.; et al. Variations of Inhalation Risks during Different Heavy Pollution Episodes Based on 3-Year Measurement of Toxic Components in Size-Segregated Particles. *Sci. Total Environ.* **2023**, *880*, 163234.

6. Lin, C.C.; Chen, S.J.; Huang, K.L.; et al. Characteristics of Metals in Nano/Ultrafine/Fine/Coarse Particles Collected Beside a Heavily Trafficked Road. *Environ. Sci. Technol.* **2005**, *39*, 8113–8122.
7. Xu, H.H.; Wang, Y.S.; Wen, T.X.; et al. Size Distributions and Vertical Distributions of Water Soluble IONS of Atmospheric Aerosol in Beijing. *Environ. Chem.* **2007**, *26*, 675–679. (in Chinese)
8. Li, X.R.; Wang, G.A.; Li, D. Particle Size Distribution and Source Analysis of Inorganic Elements in Atmospheric Aerosol in Xinglong Base Station. *J. Cap. Norm. Univ. (Nat. Sci. Ed.)* **2018**, *39*, 45–51. (in Chinese)
9. Allen, A.G.; Nemitz, E.; Shi, J.P.; et al. Size Distributions of Trace Metals in Atmospheric Aerosols in the United Kingdom. *Atmos. Environ.* **2001**, *35*, 4581–4591.
10. Wang, J.; Xu, M.; Lou, T.; et al. Size Distribution and Health Risk Assessment of Heavy Metals in Atmospheric Particulate Matter during Heating Period in the Suburb of Cangzhou. *Environ. Pollut. Control* **2022**, *44*, 335–341. (in Chinese)
11. Yang, Y.; Wang, Y.; Xu, H.; et al. Characterization of Metallic Elements of Atmospheric Aerosols at the Summit of Mount Tai. *J. Instrum. Anal.* **2008**, *27*, 390–395. (in Chinese)
12. Geng, G.; Liu, Y.; Liu, Y.; et al. Efficacy of China's Clean Air Actions to Tackle $PM_{2.5}$ Pollution between 2013 and 2020. *Nat. Geosci.* **2024**, *17*, 987–994.